COMPUTATION OF CORROSION DISTRIBUTION OF REINFORCING STEEL IN CRACKED CONCRETE

S.C. Kranc and A.A. Sagüés
Department of Civil and Environmental Engineering
University of South Florida
Tampa, Florida 33620

ABSTRACT

Cracks in concrete may cause early localized chloride ingress and the initiation of rebar corrosion. Local corrosion can be aggravated by macrocell coupling with nearby rebar in sound concrete. Computations based on a detailed finite difference model incorporating polarization characteristics of the steel and oxygen transport through the concrete have been utilized to assess the extent of corrosion possible in cracked concrete. Butler-Volmer kinetics are assumed to describe the polarization at the steel concrete interface. This investigation presents both qualitative and quantitative information concerning the distribution of corrosion in typical reinforced concrete arrangements, as a function of system parameters that include concrete resistivity, concrete cover, crack dimensions, and steel condition. The model predicts local corrosion rates at every point of the steel assembly. Applications of the modeling results to field studies to aid in the prediction of durability are discussed.
Keywords: Corrosion computation, concrete, crack, modeling, macrocell.

INTRODUCTION

Cracks that develop early in the life of a reinforced concrete structural element can facilitate the development of active corrosion [1,2,3]. The scope of this discussion will be limited to the case of structural cracks perpendicular to the reinforcing steel bars, likely to promote highly localized corrosion. Cracks that develop later in the life of the structure caused by the products of corrosion are also of interest but will not be treated here.

In marine service, the presence of a critical concentration of chloride ions is necessary for depassivation of the steel reinforcing to occur. Early cracks in vertical pilings or columns located in the region of the splash zone are of particular concern because the surface concentration of chloride ions is high and the crack may open a direct path to the rebar. The transport of oxygen may also be enhanced. Actual transport of both chloride ions and oxygen in the crack is complicated by the fact that the crack may not be filled with water but rather involve a partially filled, bridged system, capable of quickly transporting both chlorides (in the liquid phase) and oxygen (gas phase).

The following sequence of events is envisioned: A short time after the crack appears, the space inside is at least partially filled with water. Even if this water is not initially saline, it soon becomes so due to marine exposure. As the chloride concentration at the steel surface reaches a critical concentration, depassivation

Return to Table of Contents

occurs and a period of active corrosion begins at a small region where the crack meets the steel. A new distribution of electrical potential, current flow, and oxygen concentration evolves inside the concrete to support this localized active corrosion, and results in the formation of a corrosion macrocell. If the concrete is oxygen rich initially, a relatively high rate of corrosion is possible, and some time elapses before a steady state is reached with regard to potential and oxygen concentration. That steady state also will reflect the enhanced transport of oxygen to the corroding region on the steel rebar. During the ensuing period of corrosion propagation, the steel is weakened by loss of section, but the region of active corrosion may not grow substantially into the surrounding steel since some degree of local cathodic prevention may occur. The concrete cover may develop additional cracking later, as the products of corrosion swell at the steel-concrete interface.

Corrosion localization poses an important question as to which deterioration process may first limit the service life of a structure. Active corrosion in an uncracked structural element can be relatively uniform and corrosion-induced concrete cracks and spalls are the expected form of early structural deterioration. It is of considerable interest to know whether, in the case of preexisting cracks, localized corrosion could instead cause early damage by local acute loss of rebar cross section and consequent mechanical failure. This can be achieved by examination of the factors responsible for localized corrosion under these circumstances.

The purpose of this paper is to present a computational model for the corrosion macrocell that develops as a result of local activation after chloride intrusion through a crack in the concrete cover. Semiquantitative comparisons are made between the results of this investigation and existing experimental results [1]. The effort is restricted to computing the distribution of corrosion. The effect of the crack on chloride intrusion and the later development of corrosion-induced damage will be addressed elsewhere.

MODEL DEVELOPMENT

To formulate a computational model, the following scenario is adopted. The concrete is initially cast crack free and with a negligible concentration of chloride ions. The reinforcing steel is in a uniform, passive state, with a small anodic current balanced by consumption of oxygen at the steel. The oxygen concentration throughout the concrete is nearly equal to the concentration at the surface, since little consumption actually occurs. The concrete is then placed in marine service and chloride ions begin a slow transport from the outer surface of the concrete. Early in the life of the component structural cracks form and extend to the rebar depth. After a relatively short time the chloride concentration increases to critical levels near the crack-rebar intersection and active corrosion soon begins there. The present discussion, is limited to the period of time after local corrosion initiation has occurred.

The computation of corrosion propagation for reinforced concrete with known areas of depassivation has been discussed elsewhere [4-6]. Briefly, in the

Return to Table of Contents

concrete, the governing equations for the diffusion of oxygen and the electrical potential in the concrete are

$$\nabla D(\nabla C) = 0 \quad (1)$$

$$\nabla \sigma(\nabla E) = 0 \quad (2)$$

where D and C are the oxygen diffusivity and concentration, respectively, and σ and E are the electric conductivity of the concrete and E the electric potential.

At the reinforcing steel-concrete interface, boundary conditions are dictated by ongoing electrochemical reactions. Butler-Volmer [4-6] kinetics are assumed for oxygen reduction in the passive region and in the active region both anodic and cathodic reactions are presumed to occur. The assumed anodic reaction is iron dissolution to ferrous ions. Reverse reactions are neglected, as is the evolution of hydrogen. The metal dissolution and oxygen consumption reactions produce currents at the concrete-rebar interface that can be described by:

$$i_a = i_{0a}\, e^{(E_{0a}-E)/\beta_a} \quad (3)$$

$$i_c = i_{0c}\, \frac{C}{C_0}\, e^{(E-E_{0c})/\beta_c} \quad (4)$$

for the cathodic and anodic reactions (denoted with subscripts c and a, respectively). These equations are formulated in terms of local current densities and are functions of the exchange current density, i_0, the Tafel slope, β, and the equilibrium potential E_0. E is the difference of potential between the electrolyte directly in contact with the metal and the metal (see note on sign convention in Table I). The metal itself is considered as an equipotential surface by virtue of its high electric conductivity.

Applying Ohm's law at the surface (with appropriate sign convention):

$$\frac{\partial E}{\partial n} = \frac{1}{\sigma} \sum i \quad (5)$$

where n is the normal to the surface considered. Likewise, the equivalent current density due to the consumption of oxygen is given by Fick's first law by:

$$\frac{\partial C}{\partial n} = \frac{i_c}{4FD} \quad (6)$$

The factor 4 appears as the number of electrons transferred in the oxygen reduction reaction ($O_2 + 2H_2O + 4e \rightarrow 4OH^-$) and F is Faraday's constant.

To formulate a solution to the governing equations, conventional finite difference modeling has been applied. The boundary conditions at the steel-concrete interface are nonlinear and implicit, requiring an iterative solution at each computational step. The procedure is detailed in Reference [7].

Return to Table of Contents

The method outlined above has been applied to calculate the initial corrosion state of the concrete element (passive steel, uncracked concrete), as well as the final quasi-equilibrium state which results after some part of the bar becomes active and sufficient time has elapsed for the oxygen distribution profile to develop everywhere in the concrete. A similar procedure has been used to model the evolution of the potential and concentration of oxygen with time. In this case, the equation for the oxygen profile was written to include time-dependent terms and solved by a forward difference scheme in time.

RESULTS

For the purpose of the present discussion, a small laboratory-scale prismatic specimen similar to that used by Raupach [1] was chosen for modeling.

The modeled configuration is shown in Figure 1. The test rebar was simulated in the calculations as having a square cross section, 1.2 cm (0.47 in) on a side, and running continuously for the entire length of the specimen. Cover dimension was 1.5 cm (0.59 in). The model dimensions were 15 cm (5.91 in) wide by 69.6-cm (27.4 in) long by 9.6 cm (3.78 in) thick with a small active region 1.8 cm (0.71 in) long, assumed here to extend circumferentially around the rebar. The computations were performed under the assumption of insulation to the flow of oxygen on all sides except the top. The parameter values used in calculations are given in Table 1. The values of the electrochemical parameters are representative of conditions experienced during corrosion of steel in concrete [6]. The concrete properties [8] were chosen to represent a "dry" condition with high effective oxygen diffusivity and high concrete resistivity, $\rho=\sigma^{-1}$, (Condition 1, $D=10^{-3}$ cm^2/sec, $\rho=10^5$ Ω-cm), an intermediate condition (Condition 2, $D=10^{-4}$ cm^2/sec, $\rho=10^4$ Ω-cm) and a "moist" condition with low oxygen diffusivity and low resistivity (Condition 3, $D=10^{-5}$ cm^2/sec, $\rho=10^3$ Ω-cm). Note: 2×10^{-7} cm^2/sec = 1 in^2/year.

Several cases have been modeled as outlined below. The prism was assumed to have been initially uncracked, in a steady state with all the steel surface in the passive condition. Crack formation and chloride ingress were assumed to have taken place suddenly, causing immediate activation of the small central region.

Case A) The system (with intermediate concrete Condition 2) is in the state corresponding to the moment immediately after activation of the small anodic region. The concentration of oxygen in the bulk of the concrete is still that of the previous totally passive initial steady state. Thus, as corrosion begins, the concentration of oxygen is still relatively high everywhere. Oxygen transport resulting from the crack itself is ignored. The computed instantaneous corrosion current from the active region is 3.6×10^{-4} A, for a corrosion current density of 39 μA/cm^2 average on the active region surface.

Return to Table of Contents

TABLE 1: PARAMETERS USED IN COMPUTATIONS

CONCENTRATION OF O_2 AT WALL: $3x10^{-7}$ moles/cm^3

REACTION PARAMETERS	i_0 amp/cm^2	E_0 mV	β mV
IRON DISSOLUTION	$1.0x10^{-13}$	840	60
OXYGEN REDUCTION	$1.0x10^{-8}$	-260	120

Notes:

1. All potentials are in the Saturated Calomel Electrode scale, but referred to the metal. Thus, with this convention, the oxidation reaction rate increases as the potential becomes less positive. The sign convention is reflected in the equilibrium potential ranking shown in the table for the various reactions.

2. Reverse reactions (iron reduction, etc.) are considered negligible at the potentials of interest.

3. The effective concentration of O_2 is expressed in moles of O_2 per cm^3 of pore water in the concrete. The values of D selected for computation reflect that choice of concentration units. Other units for the concentration of O_2 (for example, moles per cm^3 of concrete) can be used by appropriately adjusting the value of the effective diffusion coefficient.

Case B) This case models the time-dependent response of the system (also for concrete Condition 2), beginning from the state described in (A), whereby the oxygen concentration and potential relax toward a new terminal steady state. The oxygen transport along the crack is again ignored. The corrosion current decreases and approaches a terminal value as shown in Figure 2 over a period of a few hours, which is on the order of the characteristic time $t = (1.5cm)^2/D \approx 2x10^4$ sec for diffusion of oxygen through the concrete cover. Residual relaxation of the oxygen concentration continues to occur over a much longer time frame as the oxygen concentration profile far from the corroding spot settles into the terminal configuration. Comparable reductions of corrosion intensity with time have been reported in experimental studies [1].

Cases C1, C2, and C3) Case C2 corresponds to the terminal state resulting from the process described in Case B, also ignoring transport of oxygen from the crack. The corresponding cases for concrete Conditions 1 and 3 were computed in Cases C1 and C3, respectively. The corrosion currents from the active region in cases C1, C2, and C3 are shown in Figure 3 as a function of concrete resistivity and diffusivity. The corrosion current varies only slightly as the concrete condition changes from “moist” to “dry.” The calculations assumed constant size of the active region and constant polarization parameters. Under those conditions, corrosion severity would be expected to decrease when

Return to Table of Contents

electrolytic coupling of the anodic (active) and cathodic (passive) rebar regions become poorer as a result of increasing concrete resistivity. Conversely, corrosion severity would increase as oxygen availability became better in dryer concrete. The overall trend indicates that the effect of decreased coupling was approximately balanced by that of increasing oxygen diffusivity.

A macrocell current density $i_m = i_a - i_c$ along the rebar can be defined as the difference between the local anodic and passive current densities. Figure 4 shows i_m as a function of distance along the rebar for Cases C1-C3. Integrating the macrocell current density over the surface of a given rebar segment gives the macrocell current for that segment. Figure 5 shows the ratio of the macrocell current of the active steel segment to the corrosion current of the same segment for Cases C1-C3. While the corrosion current is nearly the same in all three cases, the macrocell curent ranges from being nearly equal to the corrosion current ("moist" condition) to about 1/10 of it ("dry" condition). This decrease of macrocell effect is also observable in Figure 4, which reveals as well the shorter throwing power of the galvanic couple as the concrete resistivity increases [9].

Cases D1, D2, and D3) The computations described in C1-C3 were repeated, assuming this time that the crack dramatically enhances the transport of oxygen, keeping the concentration in the crack plane always equal to that of the outside concrete surface. The computed corrosion currents of the active zone are shown in Figure 3, showing an increase over Cases C1-C3 due to oxygen enrichment in the region surrounding the corroding spot. The increase was less pronounced for the "drier" concrete conditions since oxygen availability in those cases (by bulk diffusion of oxygen) was already good. Figure 5 shows that the ratio of macrocell to corrosion current was not significantly altered by the assumption of enhanced oxygen transport at the crack. It should be noted, however, that many potentially important processes not considered in the computations may progress in the crack itself, for example transport of corrosion products away from the active region.

The dimensions of the system were chosen to permit semiquantitative comparison of the computed behavior with experimental results reported by Raupach [1]. That investigator used a concrete specimen 70 cm (27.6 in) long that was subjected to three point loading to induce cracking. The specimen was 10 cm (3.94 in) thick and 15 cm (5.91 in) wide with rebar cover a parameter of the experiment. All of the outer surfaces of the concrete were insulated from the transport of oxygen and moisture except the top. A segmented, 1.4-cm (0.55 in) diameter rebar was located at the top and a corresponding continuous rebar was located at the bottom. The crack extended to a 2-cm (0.79 in) section of bar which was then depassivated by wetting with a chloride salt solution. The rest of the rebar on either side consisted of separated but interconnected segments 7.5 cm (2.95 in) long. After an interval of time, the macrocell strength was determined by measuring the net electronic current from each sector of the rebar. The macrocell current distributions reported in Figure 4 and also those for the D series of computations were integrated over portions of the bar length to approximately match the experimental segment arrangement. Comparison of

Return to Table of Contents

the computed and experimental macrocell currents is shown in Table 2.

As seen in Table 2, reasonable agreement was obtained between the experimental values and the computations for conditions near the center of the ranges assumed. This agreement is not an absolute model validation since the choice of other important parameters such as the polarization constants has not been tested. Nevertheless, the comparison shows that the model reproduces the main macrocell current distribution trend and that it may be a useful tool to examine the comparative effect of system variables.

The calculations with and without enhanced oxygen availability ("C" vs "D" cases) at the crack showed that oxygen transport through the crack itself may aggravate corrosion, but to a limited extent. This finding suggests that attempts at remediation by crack impregnation are not likely to dramatically reduce the corrosion rate by limiting oxygen access (crack impregnation may nevertheless hinder future chloride ingress and have a positive effect if corrosion has not yet started). The effect of oxygen transport when the active zone is larger should be nevertheless investigated in more detail since under those conditions bulk oxygen transport may be less important.

TABLE 2. COMPARISON OF COMPUTED AND EXPERIMENTAL* MACROCELL CURRENTS

Segment** (start -end distance from bar center)	Experi-mental*** (μA)	Computed (μA)					
		C1	C2	C3	D1	D2	D3
Central	200	34	206	237	34	208	451
3-10.5 cm	45	11	54	40	11	56	80
11.5-19 cm	30	3.4	27	39	3.4	27	74
20-27.5 cm	20	2.3	17	38	2.3	21	71

*From Ref. [1], concrete with 300 kg/m^3 (508 pcy) OPC, w/c=0.6, stored at 20^{o}C, 80% R.H., age 29 days.

** Central segment was ≈ 2cm (0.79 in) wide.

***Average of segments to left and right of center.

The most important effects of the crack presence early in the life of the structure appear to be the development of localized corrosion, and its enhancement by macrocell coupling. The calculations and the previous experimental evidence indicate that corrosion localization in the cm range at the crack-rebar intersection may lead to significantly high corrosion rates. Faradaic conversion of the active segment currents into metal loss shows that, if the corrosion rates remained at the levels corresponding to cases C2 or D2, the active rebar segment would lose much of its cross section in a few years. Under those conditions, early cracking could raise the possibility of failure by

Return to Table of Contents

mechanical overload in a relatively short time. The potential for similar occurrences with combinations of concrete properties and cover dimensions representative of marine bridge substructure conditions is being examined by application of the model to ongoing investigations.

CONCLUSIONS

A computational model has been formulated to assess the strength of the macrocell associated with steel corrosion near cracks in reinforced concrete. Initially the corrosion rate is relatively high due to oxygen levels in the concrete. In time the corrosion process achieves a relatively steady state condition.

Semiquantitative comparison was made to existing experimental data. Although the model configuration was not identical to the experimental specimen and some physical parameters were estimated, the experimental corrosion strength and macrocell distribution were compatible with the computations. It appears reasonable to apply this method to assessing the importance of early cracks in structural elements in service.

The calculations showed that oxygen transport through the crack itself may aggravate corrosion, but to a limited extent. This finding suggests that attempts at remmediation by crack impregnation are not likely to dramatically reduce the corrosion rate by limiting oxygen access (this conclusion might be different if the corroding area were larger).

ACKNOWLEDGMENTS

This work was partially supported by the Florida Department of Transportation (FDOT) and Academic Computing Services of the University of South Florida (USF). The opinions, findings, and conclusions expressed here are those of the authors and not necessarily those of any sponsor.

REFERENCES

1. M. Raupach, Construction and Building Materials, Vol. 10, p. 329, 1996.

2. N.M. Wilkins and P.F. Lawrence, “The corrosion of steel reinforcements in concrete immersed in seawater,” p.119 in In Corrosion of Reinforcement in Concrete Construction, A.P. Crane Ed., Ellis Horwood Publishers, Chichester, 1983.

3. Y. Ohno, S. Praparntanatorn, and K. Suzuki, “Influence of Cracking and Water Cement ratio on Macrocell Corrosion of Steel in Concrete,” p.24 in in Corrosion of Reinforcement in Concrete Construction, C.L. Page, P.B. Bamforth and J.W. Figg, Eds., The Royal Society of Chemistry, Cambridge, 1996.

Return to Table of Contents

4. S.C. Kranc, and A.A. Sagüés, "Computation of Corrosion Macrocell Current Distribution and Electrochemical Impedance of Reinforcing Steel in Concrete," in Computer Modeling in Corrosion, ASTM STP 1154, R.S. Munn, Ed., American Society for Testing and Materials, Philadelphia, PA p.95, 1992.

5. S. C. Kranc and A.A. Sagüés, Calculation of Extended Counter Electrode Polarization Effects on the Electrochemical Impedance Response of Steel in Concrete," p. 365 in Electrochemical Impedance: Interpretation and Analysis, ASTM STP 1188, D.C. Silverman, J.R. Scully and M.W. Kendig, Eds., American Society for Testing and Materials, Philadelphia, PA 1993.

6. S.C. Kranc, and A.A. Sagüés, Corrosion, Vol.50, p.50, 1994.

7. S.C. Kranc and A. A. Sagüés, J. Electrochem. Soc., Vol 144, p. 2643, 1997.

8. K. Tuutti, "Corrosion of Steel in Concrete" (ISSN 0346-6906), Swedish Cement and Concrete Research Institute, Stockholm, 1982.

9. A. A. Sagüés, S.C. Kranc, and F. Presuel-Moreno, "Advanced Computational Model for Sacrificial Cathodic Protection of Partially Submerged Reinforced Concrete Marine Footers," p.1, in Repair and Rehabilitation of Reinforced Concrete Structures: The State of the Art, W.P. Silva-Araya, O. T. de Rincon, and L. Pumarada O'Neill, Eds., American Society of Civil Engineers, Reston, VA, 1998.

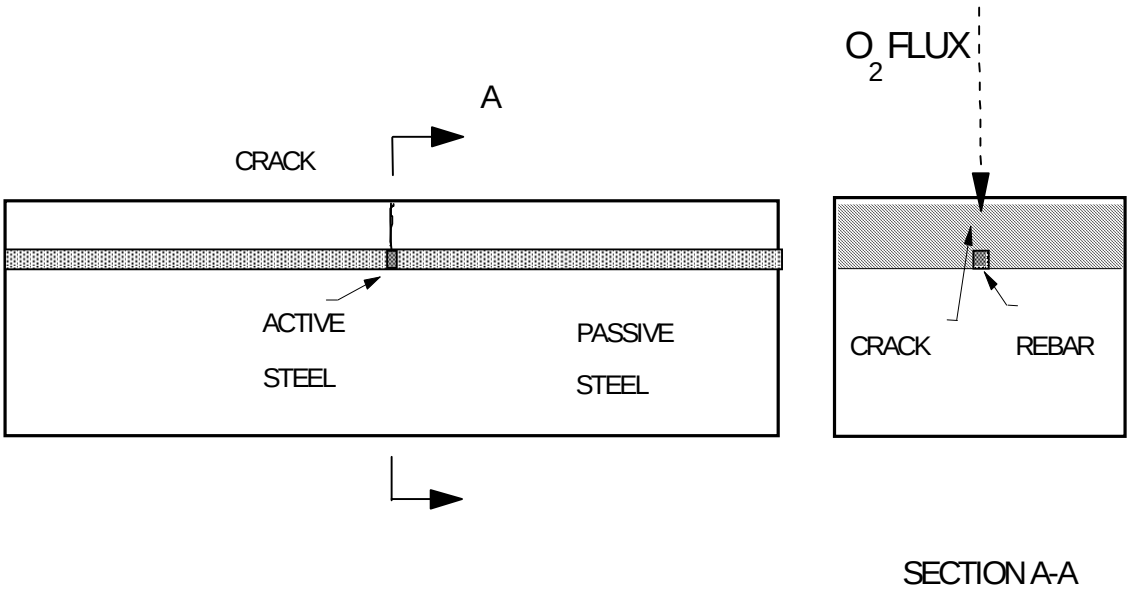

Figure 1: Configurations for model computation. Crack extends from top surface to underside of rebar as shown in Section A-A.

Return to Table of Contents

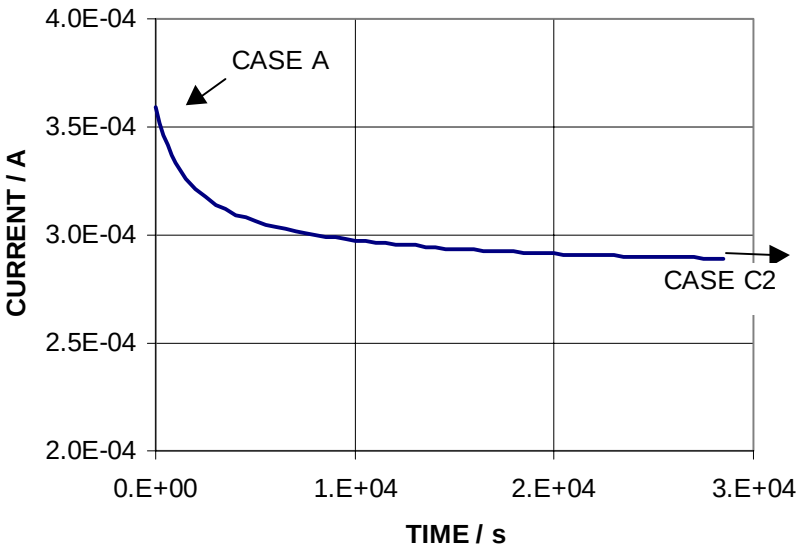

Figure 2: Initial evolution of corrosion macrocell with time. Note initial state, corresponding to Case A.

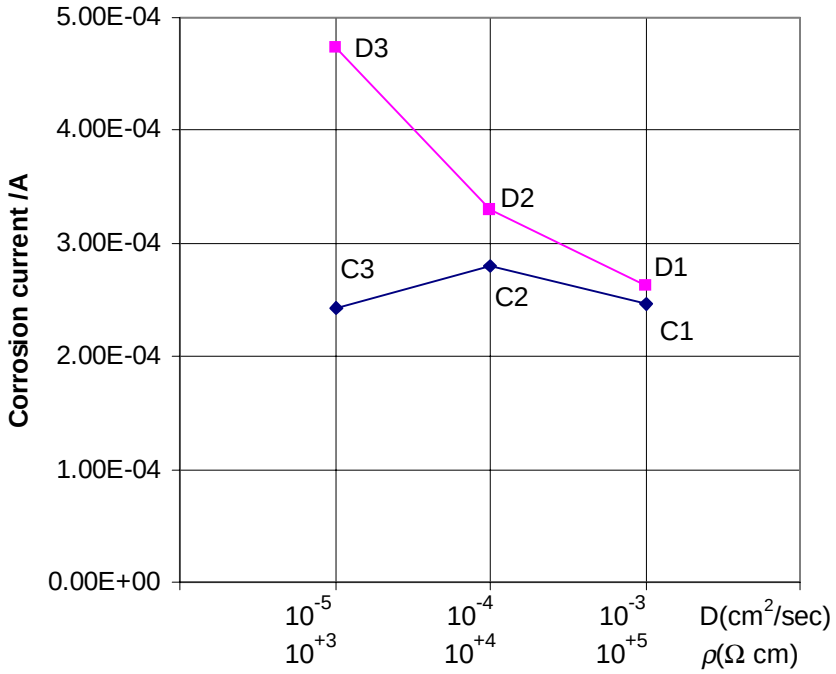

Figure 3: Corrosion current of the central active segment for cases C1-C3 and D1-D3 as function of concrete properties.

Return to Table of Contents

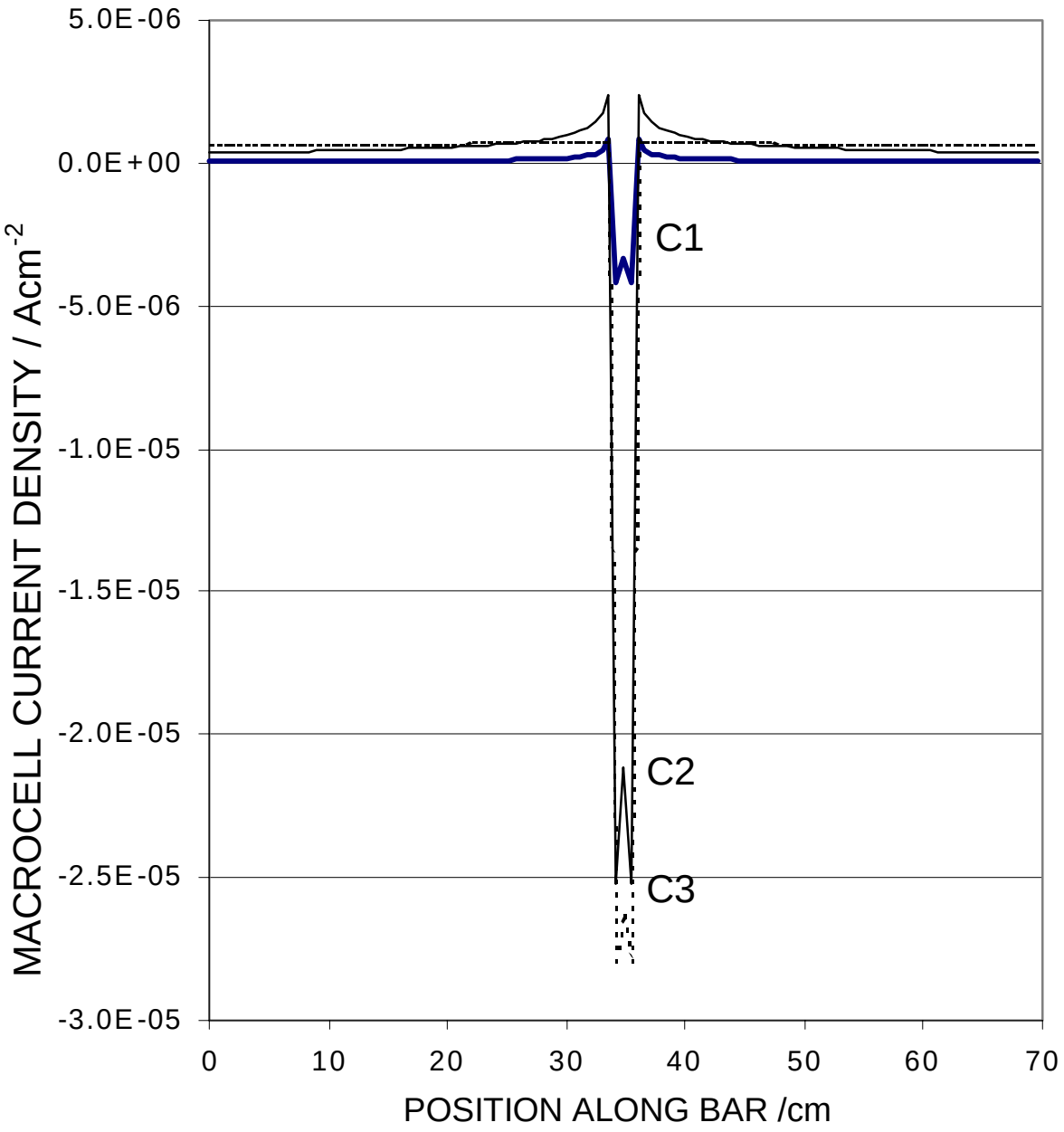

Figure 4: Macrocell current density along the bar length for cases C1-C3. Negative values mean net anodic current density.

Return to Table of Contents

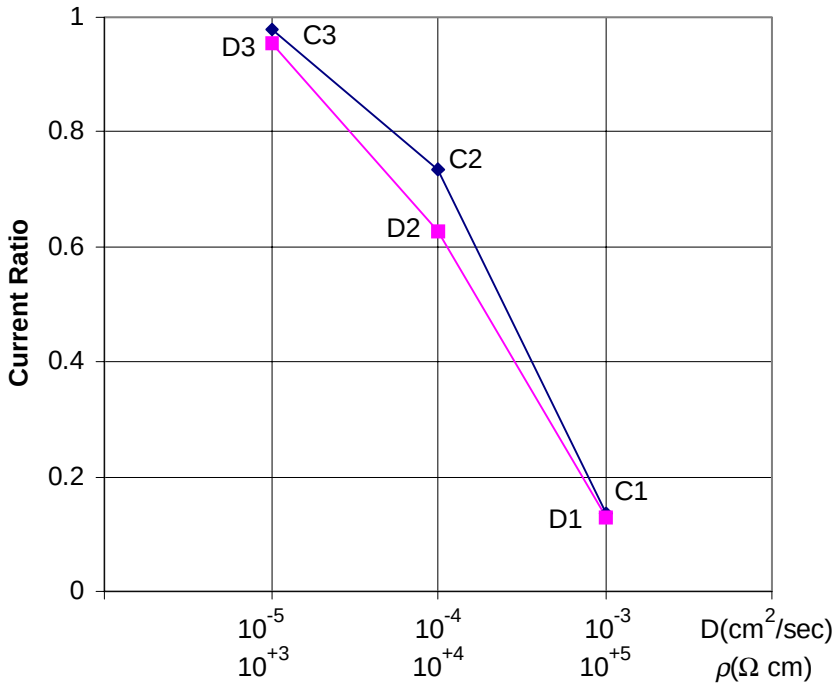

Figure 5: Ratio of macrocell current to corrosion current for the central active segment as function of concrete properties for cases C1-C3 and D1-D3.

Return to Table of Contents